Climate Dynamics (2025) 63:36
https://doi.org/10.1007/s00382-024-07512-8

ORIGINAL ARTICLE

The impact of vertical model levels on the prediction of MJO teleconnections. Part II: The stratospheric pathway in the UFS global coupled model

Chaim I. Garfinkel[1] · Zheng Wu[2,3] · Priyanka Yadav[2,4] · Zachary Lawrence[5] · Daniela I. V. Domeisen[2,6] · Cheng Zheng[7] · Jiabao Wang[8] · Andrea M. Jenney[9] · Hyemi Kim[10] · Chen Schwartz[1,11] · Cristiana Stan[12]

Received: 1 February 2024 / Accepted: 16 October 2024 / Published online: 13 December 2024

Abstract
This study continues the evaluation of the prediction of MJO teleconnections in two versions of the NOAA Unified Forecast System (UFS): prototype 5 (UFS5) and prototype 6 (UFS6). The key difference between the two prototypes is in the number of vertical layers (127 in UFS6 vs. 64 in UFS5) and model top (80 km in UFS6 vs. 54 km in UFS5), and the role of this increased resolution for the stratospheric pathway of MJO teleconnections is explored. The higher resolution prototype (UFS6) displays larger biases in its representation of tropospheric stationary waves, though both simulate a reasonable flux of wave activity entering the stratosphere. The stratospheric polar vortex in both prototypes is overly-sensitive to incoming wave activity, while both simulate a reasonable downward propagation of vortex anomalies within the stratosphere and down to the troposphere. The net effect is that both simulate the stratospheric pathway of the MJO better than has been documented for any forecasting system, though the hindcast period available for UFS differs from that used in previous studies. This allows them to predict, e.g., near-surface temperature over Eurasia with some skill on subseasonal timescales (week 3 to 5). However, this success could be the result of "two wrongs making a right", and as individual biases are fixed, skill could temporarily be reduced. Overall, the two prototypes show similar performance in simulating the stratospheric route, suggesting that in the UFS, the increase in model vertical resolution has a limited impact on the prediction of MJO teleconnections via the stratosphere.

Keywords Madden Julian Oscillation · Subseasonal predictability · Stratosphere-troposphere coupling

1 Introduction

Stratospheric variability exerts an important influence on surface weather and climate (Baldwin and Dunkerton 2001). In particular, extreme conditions of the winter stratospheric polar vortex, such as sudden stratospheric warming (SSW) (Baldwin et al. 2021) events, can lead to anomalous surface weather that can persist for several weeks. This influence is particularly pronounced over the North Atlantic / Europe region (Butler et al. 2017). In particular, SSW events are preferably followed by a negative phase of the North Atlantic Oscillation (NAO) (Charlton-Perez et al. 2018; Domeisen 2019), which is associated with cold spells in northern Europe and anomalously high precipitation in the Mediterranean region (Garfinkel et al. 2017; Kretschmer et al. 2018; Domeisen and Butler 2020). The opposite signal is generally observed in the weeks following strong vortex events (Limpasuvan et al. 2005). Hence, the stratospheric influence can enhance the predictability of surface weather following extreme stratospheric events on subseasonal to seasonal (S2S) timescales of weeks to months (Domeisen et al. 2020; Scaife et al. 2022). The stratospheric extreme events that can cause such surface impacts are, however, difficult to predict themselves in a deterministic sense on timescales longer than about a week (Domeisen et al. 2020; Chwat et al. 2022). However, certain phenomena in the climate system can change the probability of extreme stratospheric events, and hence change the odds for anomalous surface weather.

One such precursor that can change the stratospheric evolution is the Madden-Julian Oscillation (MJO), a dipole of anomalous enhanced/suppressed convection that propagates eastward across the tropical Indian and West Pacific oceans in about 40 days with a coupled circulation that

Extended author information available on the last page of the article

circumnavigates the equator (Madden and Julian 1971). Studies have shown that the MJO exerts an influence on the stratosphere. This so-called "stratospheric pathway", in turn, establishes a means by which the MJO can impact surface climate in the North Atlantic and Europe (Schwartz and Garfinkel 2017; Jiang et al. 2017). While a tropospheric pathway for this region exists (L'Heureux and Higgins 2008; Lin and Brunet 2018; Fromang and Rivière 2020), the impacts of the MJO in the Euro-Atlantic region are stronger and longer-lasting if the stratospheric pathway is activated as well (Schwartz and Garfinkel 2017; Green and Furtado 2019).

The stratospheric pathway begins with a deepened low in the western and central North Pacific during the MJO phase with enhanced convection in the West Pacific (MJO phase 6/7 as diagnosed by the RMM index of Wheeler and Hendon (2004), with largely opposite impacts for the opposite MJO phase (MJO phase 2/3). This deepened low pressure system constructively interferes with the climatological wavenumber-1 trough that is present in the North Pacific, and subsequently leads to enhanced upward propagating wave activity entering the stratosphere (Garfinkel et al. 2012, 2014). This enhanced wave activity weakens the vortex, and subsequently leads to a negative Northern Annular Mode (NAM) and NAO signal down to the surface (Schwartz and Garfinkel 2017). Further, the MJO has been shown to enhance the predictability of the stratosphere and the NAO on S2S timescales (Lin et al. 2010; Garfinkel and Schwartz 2017).

This relationship between tropical MJO convection, the Arctic stratosphere, and the extratropical surface climate is not sufficiently represented in many models. In particular, model biases in the representation of the MJO itself and its tropospheric teleconnection (Vitart 2017; Kim et al. 2018; Stan et al. 2022), in extratropical stationary waves (Schwartz et al. 2022) and in the stratospheric polar vortex (Lawrence et al. 2022), can limit the representation of this pathway in models. None of the subseasonal forecasting models considered in Schwartz et al. (2022) or in Stan et al. (2022) were able to simulate the entirety of the stratospheric pathway, though several were able to simulate the first few components of the pathway (e.g., enhanced wave flux and a weakened vortex for MJO phase 7).

A range of S2S models still use low model tops (i.e., below the stratopause) and coarse vertical resolution in the stratosphere (Domeisen et al. 2020), which is likely one of the reasons for a poor representation of stratospheric pathway teleconnections. Model intercomparison studies have shown that low-top models generally have a less well represented stratosphere with larger biases in polar vortex strength and in the frequency and predictability of stratospheric extreme events (Lawrence et al. 2022). On seasonal timescales, the pathway of tropical forcings such as the El Niño Southern Oscillation is less well represented in low-top models (Butler et al. 2016). On subseasonal timescales, a clean intercomparison where the only difference between models is the vertical resolution has not yet been possible. For example, the S2S database (Vitart et al. 2017) consists of an ensemble of opportunity, where roughly one-third of the models can be considered low-top (Domeisen et al. 2020). Hence, while models with a high model top and higher vertical resolution in the stratosphere generally exhibit a less-biased representation of the stratospheric pathway (Stan et al. 2022), it is not clear if these improvements are entirely due to the better resolution of the stratosphere, or if these improvements are due to other factors in high-top models, which often also exhibit a better representation of tropospheric processes.

In this study, we show evidence, for the first time, of a subseasonal forecasting model successfully capturing the stratospheric pathway. Further, we consider the role of vertical model resolution by contrasting the MJO stratospheric pathway in model configurations that differ primarily in vertical resolution and model top, with minimal additional changes to parameterizations.

The remainder of this paper is organized as follows: In Sect. 2 we describe the models and reanalysis data that are used in this study; results from the simulations are compared with reanalysis in Sect. 3; and we conclude with a summary and discussion of the results in Sect. 4.

2 Data and methods

2.1 Forecast models

We analyze reforecasts from two versions of the Unified Forecasting System (UFS) Coupled Model, Prototype 5 and 6 (UFS5 and UFS6), developed by the National Center for Environmental Prediction (NCEP). These prototypes were introduced in detail in Paper 1 (Zheng et al. 2024). Paper 1 also discussed the tropospheric route for MJO teleconnections and MJO prediction skill. Here, we elaborate on the main differences between these two prototypes of relevance for the stratospheric pathway: the atmospheric vertical resolution and an upgrade to the physics.

The atmospheric component in both prototypes uses the FV3 dynamical core on the cubed-sphere grid (Putman and Lin 2007; Harris and Lin 2013) at C384 ($\sim 0.25°$) horizontal resolution. Both also use the Common Community Physics Package (CCPP) for physics and land-surface parameterizations. However, the two prototypes have a different distribution and number of vertical layers: the number of levels increases from 64 with a model top at 54 km in UFS5, to 127 with a model top at 80 km in UFS6. In Fig. 1, the thickness of each model layer is shown as a function of pressure and compared between the two UFS versions. The figure also shows the layer thickness if UFS5 vertical resolution was

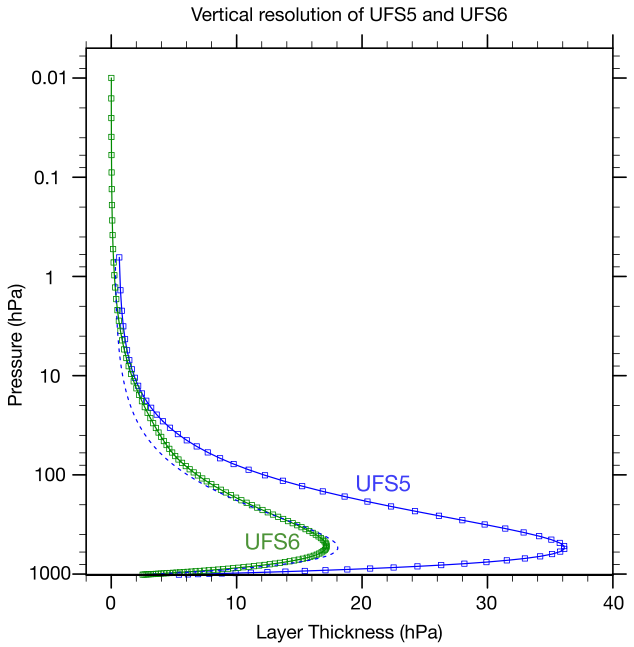

Fig. 1 Vertical resolution of UFS5 (blue) and UFS6 (green). The pressure of each model layer is represented on the y-axis, while the thickness of each layer is represented on the x-axis. The dashed line depicts the distribution as if the thickness of each UFS5 model layer is reduced to its half (doubling UFS5 vertical resolution)

simply doubled, with the thickness of each layer reduced to half of its UFS5 value. Below ~270 hPa, UFS6 resolution is slightly finer than simply doubling UFS5 resolution, while above ~270 hPa, UFS6 resolution is coarser than doubling UFS5 resolution. Overall, UFS6 vertical resolution is about double compared with UFS5 from the surface to the lower stratosphere (~100 hPa). One might hypothesize that this increase would lead to a better representation of the stratospheric pathway, and we test this hypothesis in this paper.

There are a few updates in model physics between UFS5 and UFS6. Namely, UFS5 uses the GFSv15.2 physics package while UFS6 uses GFSv16. These upgrades in GFSv16 are discussed in detail in Stefanova et al. (2022). Of these changes the most relevant is the addition of a parameterization for sub-grid scale non-stationary waves in the gravity wave drag parameterization scheme. This parameterization is intended to allow for a reasonable representation of the lower mesosphere after the lid is raised to 80 km (Holton 1982; Ern et al. 2011).

2.2 Methods

Reforecasts from April 2011 to March 2018 have been generated by NCEP for both UFS5 and UFS6. Each reforecast is initialized on the first and fifteenth of each month (168 deterministic reforecasts in total) and forecast lead time extends to 35 days. The focus of this paper is on extended boreal winter (November to March) for which 70 reforecasts in each prototype are initialized during the analysis period.

We compare the reforecasts described above with atmospheric reanalysis. We use temperature, wind, and geopotential height from the European Centre for Medium-Range Weather Forecasts (ECMWF) Reanalysis - Interim (ERA-Interim, hereafter ERA-I Dee et al. (2011)) at 1.5° horizontal resolution. Select figures have been recreated using ECMWF Reanalysis v5 (ERA5) data, and results are essentially identical. We subsample the reanalysis to match the same time period used for UFS (2011–2018).

The climatology of each prototype is defined by averaging the reforecasts that are initialized on the same day of each year (e.g. averaging all reforecasts initialized on January 1 during the period 2011–2018). A unique climatology is created for each initialization date and lead-time. Then, the anomalies are obtained as the deviation from each prototype's climatology. The same procedure is used to define a climatology and anomalies for reanalysis.

The upward flux of planetary waves is diagnosed using the meridional eddy heat flux, $v'T'$ (with v being the meridional wind, T the temperature, and the primes denoting deviations from the zonal mean). To focus on the contribution of individual wavenumber components for this upward flux, we decompose v and T by wavenumber before computing their product (e.g., $v_{k=1}T_{k=1}$ for wave-1 heat flux).

The method used for defining the MJO is similar to that in Paper 1 (Zheng et al. 2024). The MJO is defined by the real-time multivariate MJO (RMM) index (Wheeler and Hendon 2004). The RMM index is constructed from the 1st and 2nd principal components of the combined empirical orthogonal functions (EOFs) of 15°N-15°S averaged zonal wind at 850 hPa and 200 hPa and OLR. The phases and amplitude of the MJO are calculated with the RMM index following Wheeler and Hendon (2004). Active MJO events are defined as times when the observed RMM amplitude is larger than 1 standard deviation at the time when the reforecasts are initialized. There are 48 active MJO events in total during the analysis period. Lagged days of RMM phases are defined as days after the reforecast initialization time when the MJO is active in a specific RMM phase.

3 Results

In order for a model to even hope to represent the stratospheric route, it needs to reasonably simulate the following regardless of the presence of the MJO:

1. Minimally-biased tropospheric planetary waves that propagate upward into the stratosphere
2. The correct sensitivity of the stratospheric polar vortex to upward wave driving

3. Downward propagation of stratospheric polar vortex anomalies from the mid- and upper-stratosphere to the lower stratosphere where the signal then persists for months due to the long radiative timescales (Hitchcock et al. 2013)
4. Downward propagation from the lower stratosphere to the surface, with particular foci in the Euro-Atlantic sector that project onto the NAO.

Hence, we first consider whether UFS5 and UFS6 are capable of simulating these four factors independent of the MJO (Sects. 3.1 and 3.2), before considering the stratospheric pathway of the MJO specifically (Sect. 3.3) and the associated surface impacts (Sect. 3.4).

3.1 Upward troposphere to stratosphere coupling

We begin by analyzing tropospheric quasi-stationary planetary waves. Specifically, Fig. 2 shows the deviation of 500 hPa height from the zonal average in weeks 3 to 5 in NDJFM. Both UFS prototypes simulate quasi-stationary waves that are qualitatively similar to reanalysis: a ridge over the North Atlantic and Western North America, and a trough over East Asia and Hudson Bay. However, the ridge over Western North America is too weak in both prototypes, a bias similar to that evident in many S2S models (Schwartz et al. 2022). Further, the trough over Hudson Bay is too weak in both prototypes, while the East Asian trough is shifted eastward in UFS6 but does not extend far enough eastward in UFS5.

The most important components for the stratosphere of the quasi-stationary wave field are the zonal wavenumber-1 and wavenumber-2 components, as these are the waves that most easily transit the tropopause and reach the polar stratosphere (Charney and Drazin 1961; Weinberger et al. 2022). The too-weak Western North American ridge and Hudson Bay trough have implications for wavenumber-2. Namely, these biases overlay the climatological wavenumber-2 field in reanalysis (indicated in magenta), and hence the quasi-stationary wave-2 field is too weak. In contrast, wave-1 is too strong in UFS6 due to the eastward extension of the East Asia trough and North Atlantic ridge. The net effect is that quasi-stationary wave biases in the lower stratosphere are larger in UFS6 than in UFS5 (Fig. 3). Specifically, the bias in UFS6 includes a pronounced ridge over North America which projects onto the climatological wave-1 ridge. This constructive interference between the bias and the stationary waves might plausibly be related to too-much wave-1 heat flux at 100 hPa (Schwartz et al. 2022). We will demonstrate shortly that this hypothesis is confirmed.

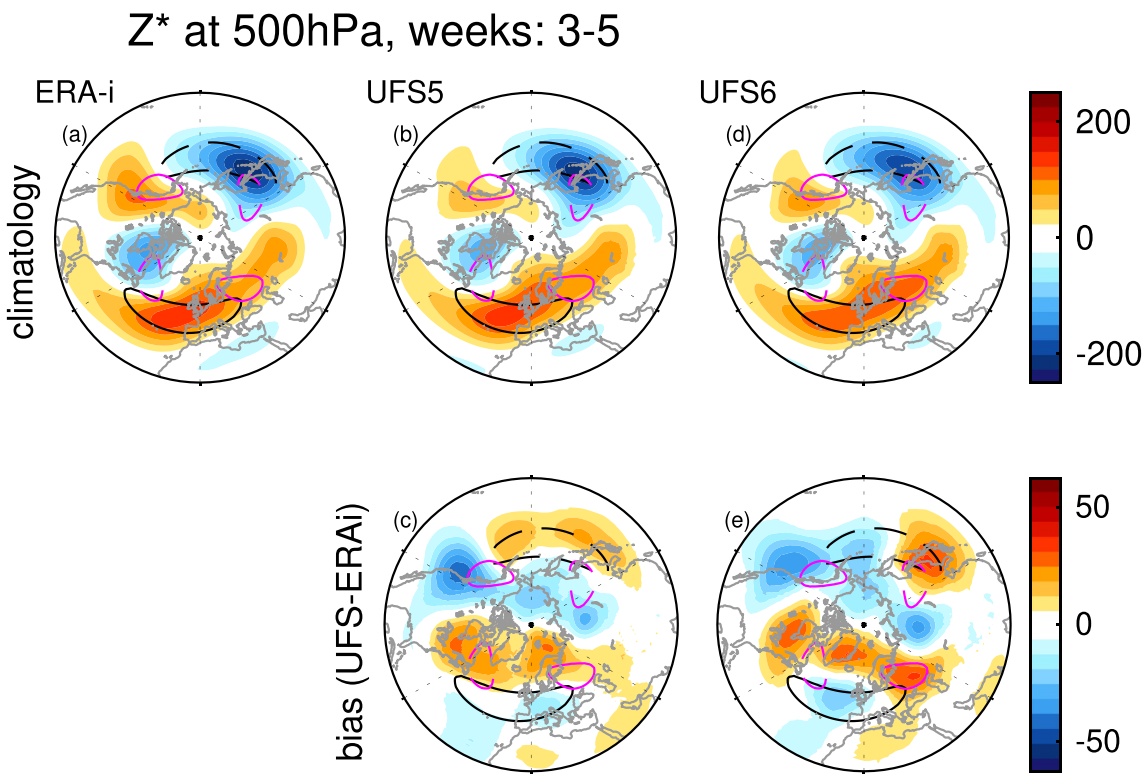

Fig. 2 Deviation of 500 hPa height from the zonal average in weeks 3 to 5 for each UFS prototype, and in reanalysis for the corresponding dates. All seventy initializations in November through March over 2011–2018 are used. Observed climatological wave-1 is indicated with black contours, and climatological wave-2 with magenta contours

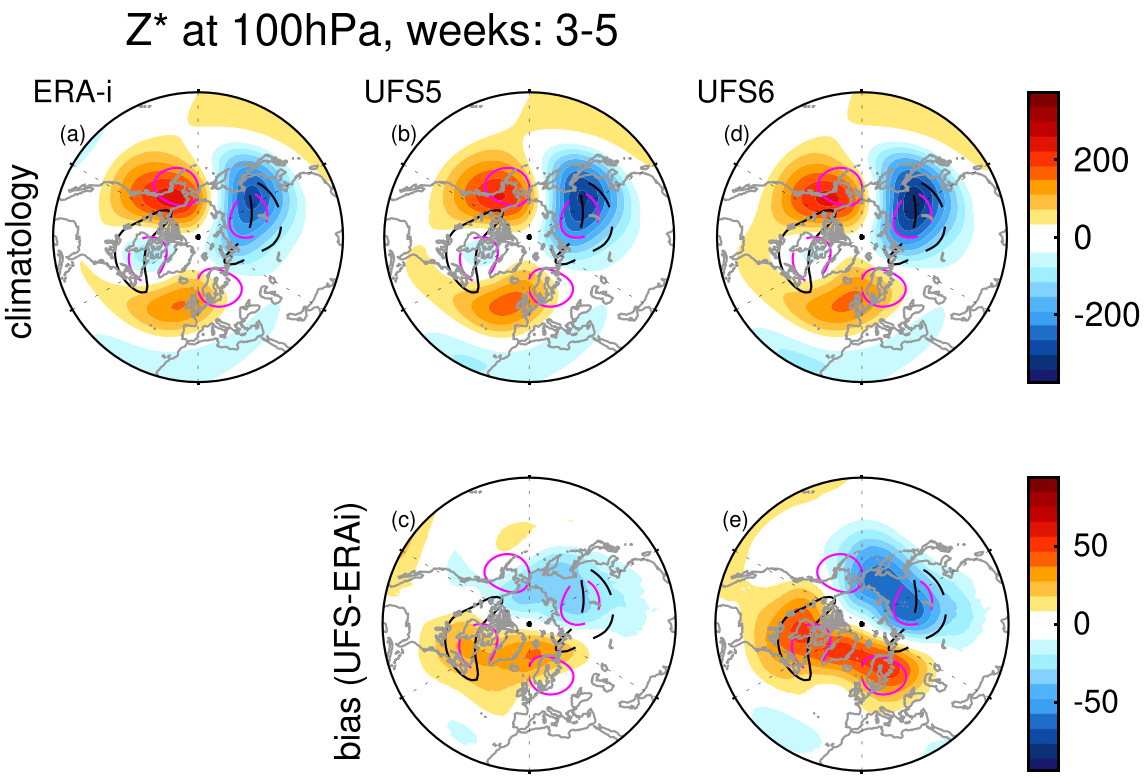

Fig. 3 As in Fig. 2 but for 100 hPa

These biases in quasi-stationary waves are reflected in the wave-driving of the vortex. Figure 4 shows the climatological wave-1 and wave-2 heat fluxes at 500 hPa and 100 hPa for each week. At both levels, UFS6 has too much wave-1 heat flux and too little wave-2 heat flux in later weeks. The too-weak 100 hPa wave-2 heat flux bias is statistically significant in December through February (not shown). UFS5, on the other hand, has smaller biases overall. Even though the relative magnitude of wave-1 versus wave-2 is biased in UFS, the sum of wave-1 and wave-2 is reasonable in both prototypes compared to reanalysis.

The too-weak wave-2 bias in the time-mean also is reflected in the spread in the representation of wave-2 at 100 hPa and 500 hPa across different initializations. Figure 5 contrasts heat flux anomalies at 500 hPa with those at 100 hPa three days later. We note that a three day lag maximizes the relationship, however results are similar for shorter or longer lags. While both UFS5 and UFS6 capture the correlation and the magnitude of the regression coefficient between tropospheric and lower-stratospheric heat flux for wave-1, UFS6 underestimates both the correlation and the regression coefficient for wave-2 (Fig. 5bf). This implies that stratospheric wave-2 in UFS6 is relatively decoupled from its tropospheric precursors. We demonstrate this explicitly in Fig. 6, which shows 500 hPa height three days before week-long periods with anomalously strong minus anomalously weak heat flux at 100 hPa. We only include forecast weeks 3 to 5 to exclude the period closest to initialization. In reanalysis, anomalously strong wave-1 heat flux at 100 hPa is preceded by a trough over the North Pacific and a ridge over the Atlantic which constructively interferes with the climatological wave-1 (indicated with a black contour; c.f. Garfinkel et al. 2010). Anomalously strong wave-2 heat flux at 100 hPa is also preceded by constructive interference at 500 hPa, and specifically with a ridge over Alaska and Scandinavia and a trough over Hudson Bay and Eastern Siberia. While both UFS prototypes qualitatively capture the features evident in reanalysis, the magnitudes are too weak, with wave-2 too-weak for UFS6 and wave-1 too weak for UFS5, even as the patterns are generally correct.

After the anomalous wave driving enters the stratosphere, it modulates the strength of the vortex. We diagnose this effect in the left column of Fig. 7, which contrasts the sum of wave-1 plus wave-2 heat flux in weeks two through four with the change in polar cap height (60 N to the pole area-weighted) at 10 hPa from one week prior to one week after the week chosen for the heat flux. For example, we contrast week 3 heat flux with the change in polar cap height between week 4 and week 2. The correlation between the metrics is similar in reanalysis and in both prototypes, however the regression coefficient is significantly weaker in reanalysis than in UFS. This implies that a given heat flux anomaly

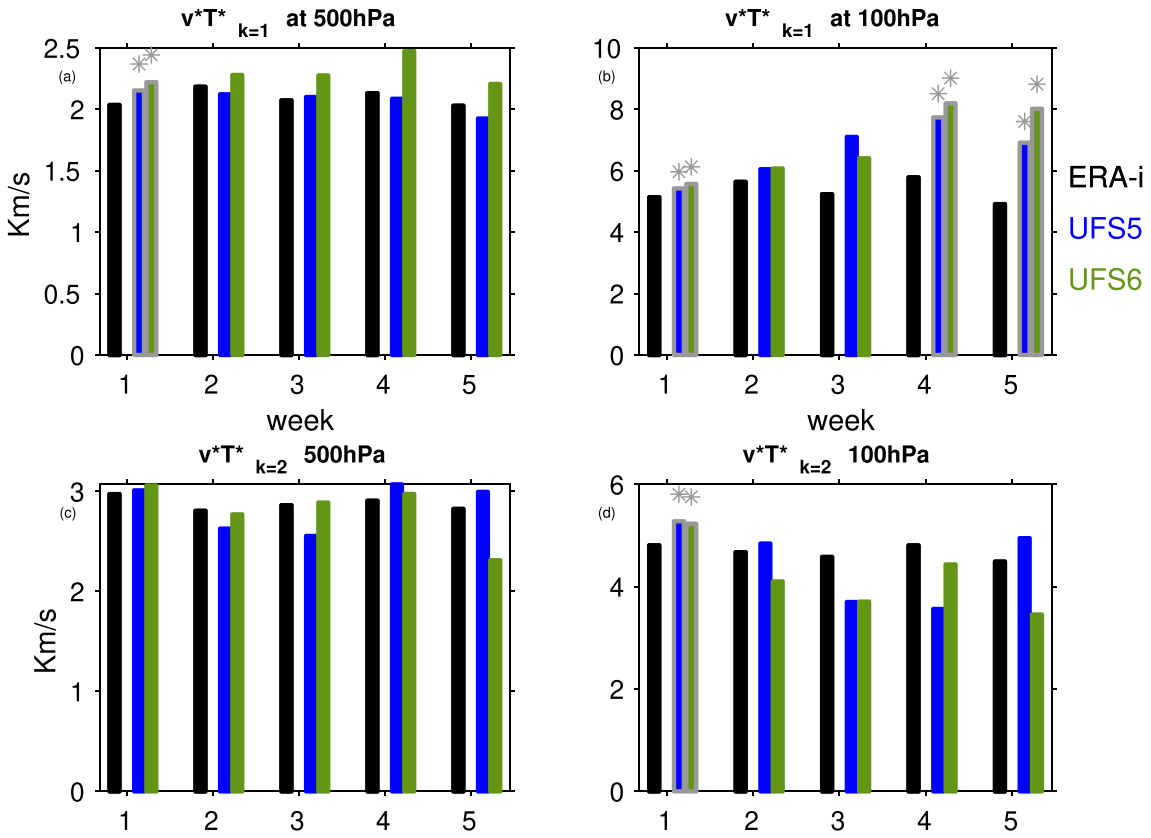

Fig. 4 Climatology of heat fluxes at 100 hPa and 500 hPa in November through March over 2011–2018. A silver outline and star indicates that the UFS climatology differs significantly from reanalysis at the 95% level using a paired t-test

has a stronger impact on the vortex in UFS than in reality. The net effect is that while UFS may underestimate the lower stratospheric heat flux induced by a given tropospheric anomaly (for example, one forced by the MJO), this too-small heat flux perturbation can still have a reasonable effect on the polar vortex due to an overly sensitive vortex in these UFS prototypes.

Overall, UFS6 struggles to capture the generation of wave-2 in the troposphere, and the polar vortex is also overly sensitive to heat flux in the lower stratosphere in both prototypes. Nevertheless, these biases are relatively less important for generating a stratospheric pathway of the MJO, as the MJO predominantly affects the polar vortex via its effect on the Aleutian Low and tropospheric wave-1 (Garfinkel et al. 2014).

3.2 Downward stratosphere to troposphere coupling

We now consider downward coupling within the stratosphere. The right column of Fig. 7 contrasts polar cap height anomalies at 10 hPa with those at 100 hPa three days later. This three day lag maximizes the relationship in reanalysis data (not shown). Higher polar cap heights at 10 hPa are associated with higher polar cap heights at 100 hPa; that is, a weakened vortex at 10 hPa precedes a weakened vortex at 100 hPa. In both UFS prototypes, this downward propagation within the stratosphere is slightly too strong as compared to reanalysis, with the difference statistically significant. It is also worth noting that the range of polar cap heights at both levels is larger in UFS, especially for negative anomalies and in UFS6.

We now assess the persistence of lower stratospheric temperature anomalies, which is needed to provide a continual exogenous forcing on the troposphere below over the following weeks. We examine this effect in the left column of Fig. 8, which contrasts polar cap temperature anomalies in weeks 2 and 3 with the corresponding polar cap temperature anomalies two weeks later. Both UFS prototypes realistically capture the persistence of temperature anomalies, and hence once the vortex is modulated, we should expect a long-lived tropospheric response.

Finally, we assess the ability of the lower stratospheric vortex anomaly to affect the tropospheric circulation in each prototype, with a particular focus over the Atlantic sector. This effect is examined in the right column of Fig. 8, which contrasts polar cap height at 100 hPa with height at 500 hPa from 55N-pole and 300E to 359E. This region corresponds

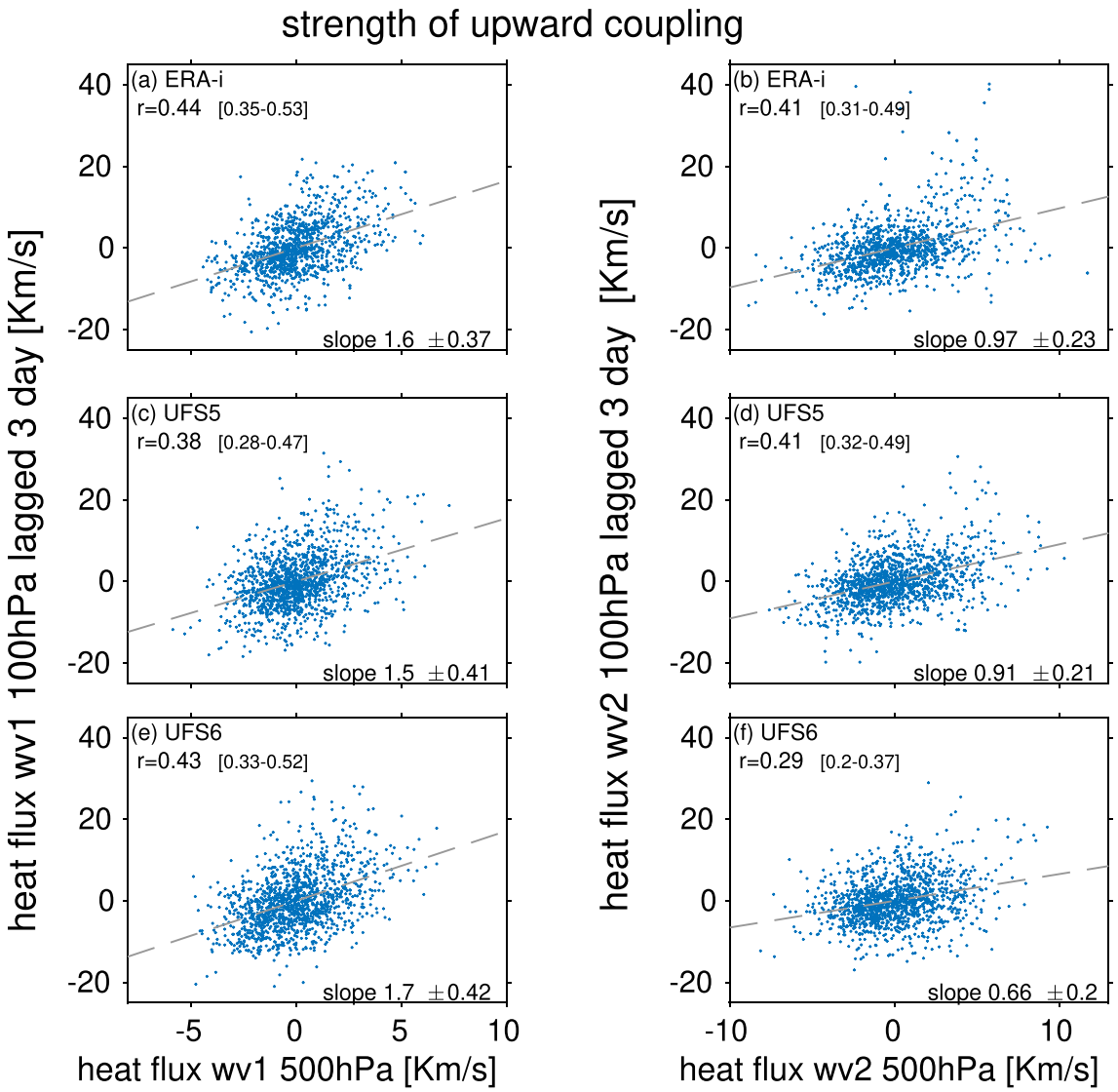

Fig. 5 Comparison of heat flux at 500 hPa with heat flux at 100 hPa three day later in weeks 3–5 in the 70 initializations from November through March. (left) wave-1; (right) wave-2. Specifically, we contrast 500 hPa heat flux from days 15 through 33 (x-axis) with 100 hPa heat flux in days 18 through 35 (y-axis) for each of the 70 initializations. The 95% confidence intervals on the slope and correlation coefficient are indicated on each panel using a Student t-test, with the reduction in degrees accounted for following equation 31 of Bretherton et al. (1999)

to the Icelandic Low node of the North Atlantic Oscillation. Both UFS prototypes perform well for this metric, though there is a hint of a too-weak impact in UFS5.

Overall, UFS performs well in capturing downward coupling within the stratosphere and down to the troposphere.

3.3 MJO teleconnections to the Euro-Atlantic sector via the stratosphere

As discussed before, the MJO can influence surface weather and climate in the North Atlantic / Europe region through a stratospheric pathway. In this section, we consider whether UFS5 and UFS6 are capable of capturing the MJO stratospheric pathway by assessing both the upward and downward coupling between the stratosphere and troposphere.

We first investigate the upward leg of the MJO stratospheric pathway. Figure 9a-i shows the time evolution of wave-1 and wave-2 meridional heat flux anomalies averaged over 40–80N, following each MJO phase in reanalysis and in each prototype during November to March. Positive anomalies of wave-1 and wave-1+2 heat fluxes at both 500 (Fig. 9a–f) and 100 hPa (Fig. 9g–i) are present in weeks 2 to 4 after MJO phases 5 in reanalysis and UFS. The potential for predictability of upward heat flux extends to subseasonal timescales: both UFS5 and UFS6 have enhanced

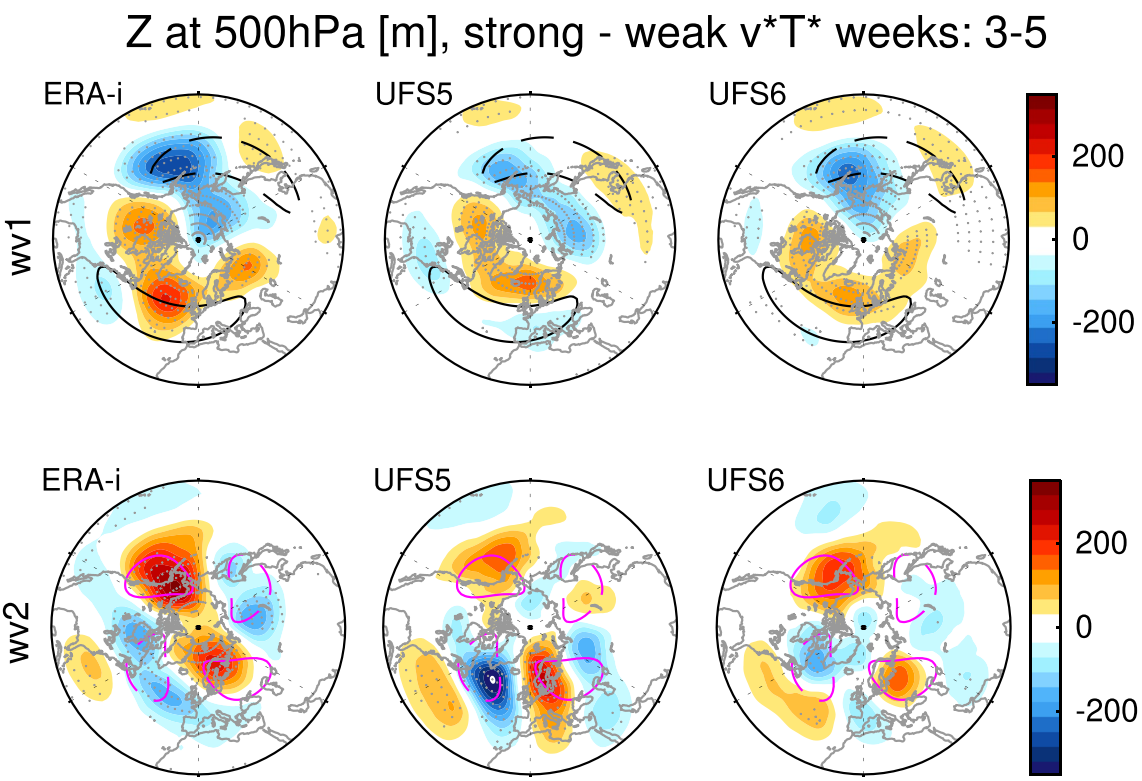

Fig. 6 Height anomalies at 500 hPa in weeks 3–5 when (top) wave-1 and (bottom) wave-2 heat flux at 100 hPa is anomalously strong or weak (anomalies exceed 8 Km/s in absolute value) three days later in November through March. Climatological wave-1 is indicated with black contours, and climatological wave-2 with magenta contours. Stippling indicates where the difference in Z500 between the strong heat flux vs. weak heat flux composites is statistically significantly different at the 95% level using a student t-test

heat fluxes at both levels 2–3 weeks following MJO phase 4. Comparing the first two rows in Fig. 9, the strong heat flux is mainly from its wave-1 component. UFS6 tends to simulate much stronger heat fluxes than reanalysis after MJO phases 4 and 5. This is consistent with the too-strong climatological wave-1 heat fluxes in the UFS6 shown in Fig. 4. This heat flux response in the troposphere precedes a strong stratospheric heat flux response: the maximum positive heat flux anomalies at 100 hPa in both prototypes are present in week 4 after MJO phase 4, i.e., it is offset by one phase relative to reanalysis (Fig. 9g–i).

Consistent with the increased heat fluxes entering the stratosphere, a weakening of the stratospheric polar vortex (Fig. 9j–l) is evident in weeks 4–5 following MJO phase 5 in ERA-I and in weeks 3–5 following MJO phase 4 in both prototypes. Both prototypes simulate the negative anomalies of the polar vortex in weeks 2–3 after MJO phases 7–8, similar to the reanalysis. Both prototypes reproduce an intensified polar vortex following MJO phases 2 to 3 as in the reanalysis, while they show the opposite responses to the reanalysis in the polar vortex strength in weeks 4–5 after MJO phase 1. Overall, the polar vortex strength is weaker after MJO phases 4–8 than that after MJO phases 2–3 in both UFS and reanalysis, however the magnitude and specific phase with peak response in UFS does not match that in reanalysis.

Further insight into the weakening of the polar vortex after MJO phases 5 and 6 compared to the strengthening after MJO phases 2 and 3 is shown with histograms of zonal-mean zonal wind at 10 hPa and 60N (U1060) in Fig. 10. It is notable that the differences in the mean polar vortex strength between MJO phases 5–6 and 2–3 in weeks 1–5 are similar in both prototypes and in the reanalysis, consistent with Fig. 9. This indicates an increased probability of an extremely strong polar vortex after MJO phases 2–3 and of a substantially weak polar vortex after MJO phases 5–6. Although UFS does not reproduce the most extremely weak polar vortex seen in reanalysis, it is able to simulate the extremely strong polar vortex events after MJO phases 2–3. Overall, Fig. 10 suggests that both prototypes simulate the distribution of polar vortex strength following MJO phases 2–3 and 5–6, with changes particularly pronounced at the positive tail of the distribution for very strong vortex events.

We next examine the downward leg of the MJO stratospheric pathway. Figure 11 shows the response of geopotential height at different pressure levels following each MJO phase. An increase of 10 hPa height averaged over the polar cap follows MJO phase 5 in weeks 3–5 (Fig. 11a-c). The

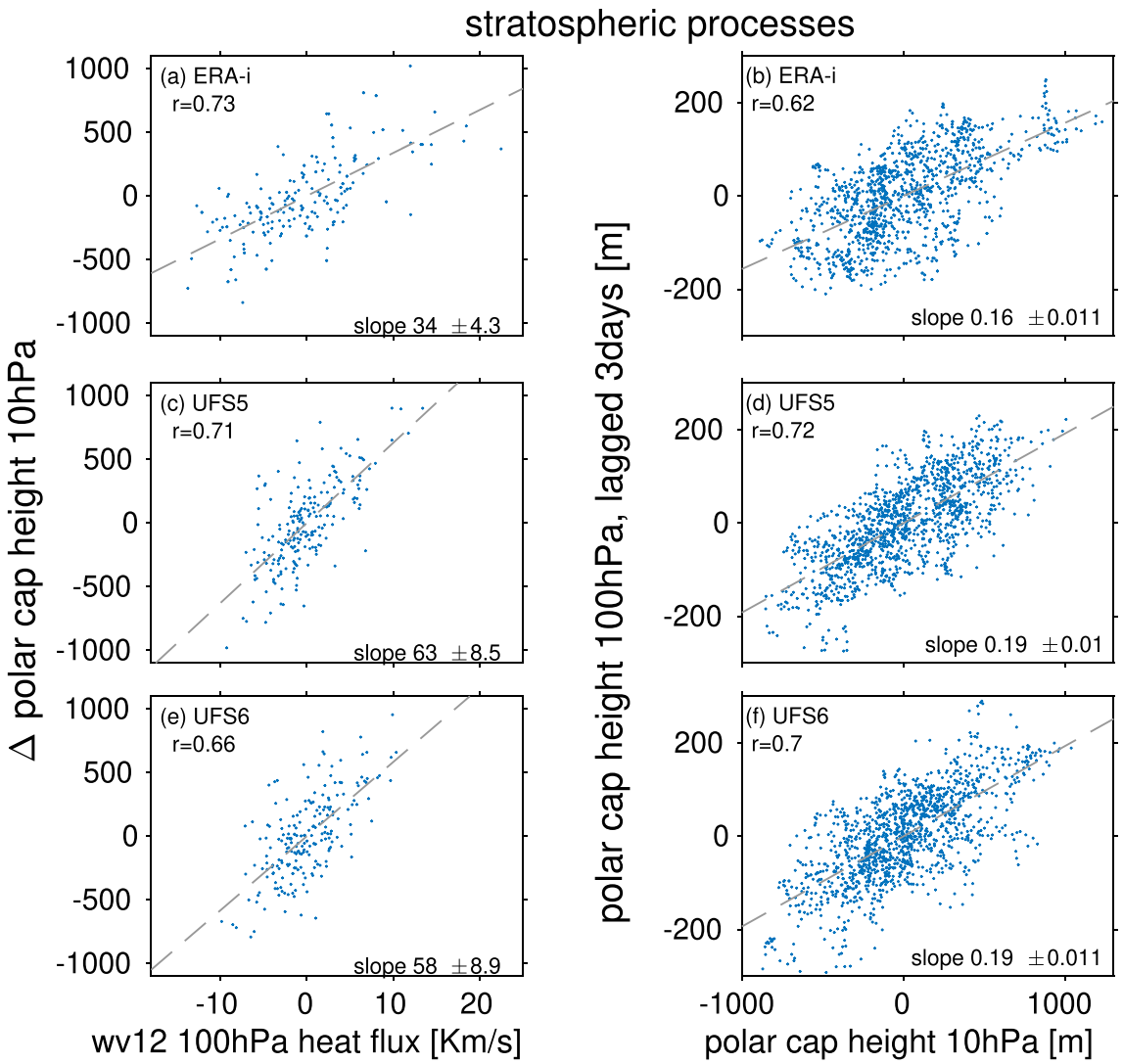

Fig. 7 (left) Comparison of weekly averaged wave-1 plus wave-2 heat flux at 100 hPa in weeks two through four with the difference in polar cap height one week before to one week after the heat flux (e.g., heat flux in week 3 compared to the difference in polar cap height between week 4 and 2). (right) Comparison of polar cap height at 10 hPa with that at 100 hPa lagged three days later in weeks two through five. Daily data is used for the right column, while weekly-mean data is used for the left column, hence there is a large difference in the number of dots

increased height indicates the Northern Annular Mode, NAM's negative phase, which corresponds to a weakening of the polar vortex in Fig. 9j-l. The magnitude and timing of the 10 hPa height response in UFS is similar to that in reanalysis though the maximum occurs following MJO phase 4 (one phase earlier than in reanalysis), consistent with the polar vortex response (Fig. 9j-l). The downward propagation within the stratosphere and to the troposphere can be seen in Fig. 11d-i. Positive polar cap 100 hPa height anomalies are present in weeks 1–3 after MJO phase 6 in the reanalysis and UFS6, while UFS5 simulates positive 100 hPa height anomalies 4–5 weeks after MJO phase 4 and underestimates the persistance of the phase 6 response. Similar positive height responses after MJO phases 5 and 6 in both prototypes and reanalysis are shown at 300 hPa, with UFS6 simulating a more positive height anomaly than the reanalysis that persists for too long. In general, the values of polar cap averaged height in the stratosphere and troposphere tend to be higher in weeks 1–5 after MJO phases 5–7 than after MJO phases 2–3 in the reanalysis and both prototypes (first three rows in Fig. 11). This NAM response is consistent with the weakening of the polar vortex evident in Fig. 9j-l and Fig. 10, and indicates the downward propagation of the stratospheric anomalies related to the MJO.

The height responses over the Euro-Atlantic sector are presented in the last row of Fig. 11, with positive anomaly indicating a negative phase of the NAO, which is often preceded by anomalously weak polar vortex events such as

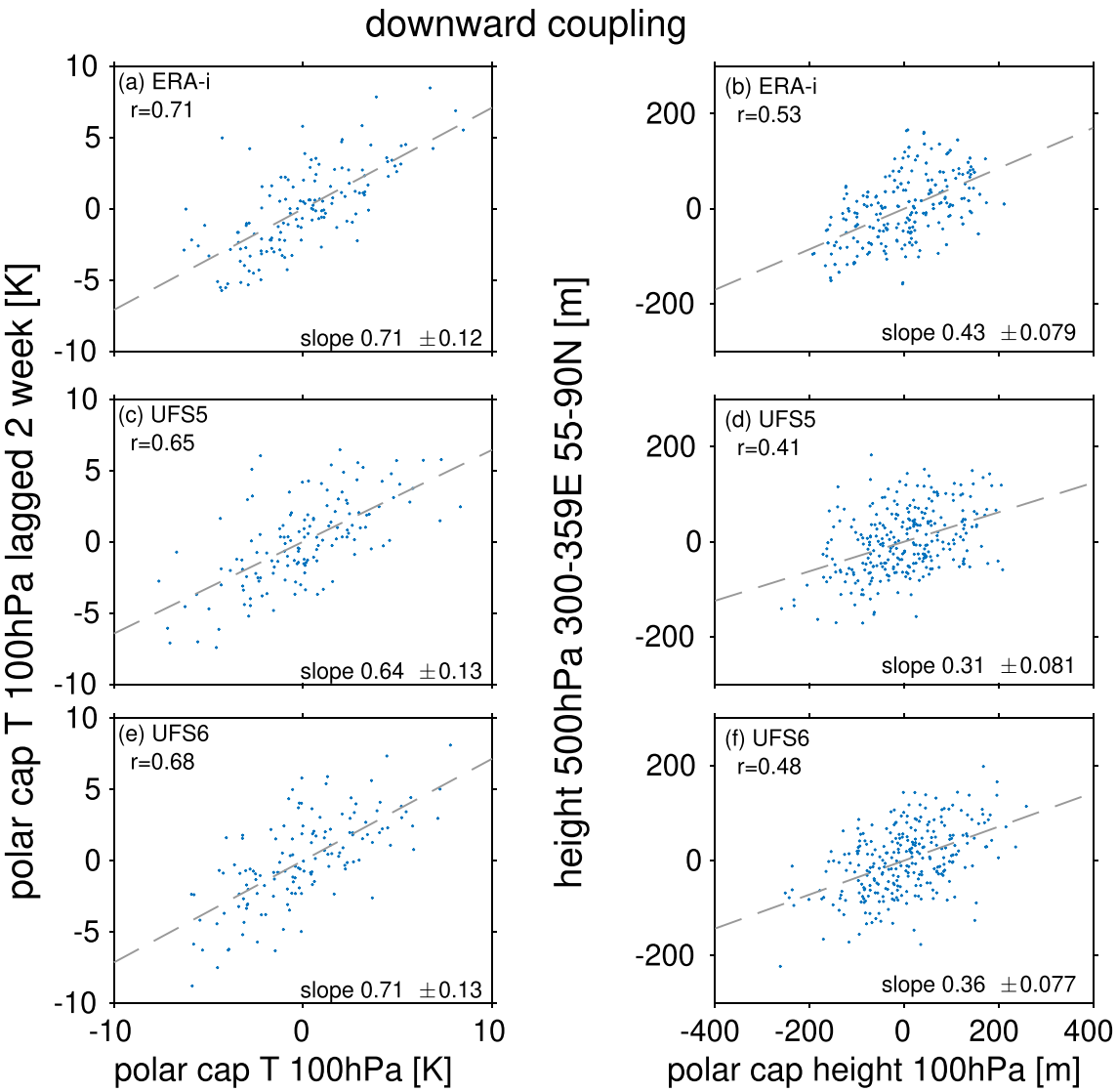

Fig. 8 (left) persistence of polar cap temperature anomalies from week 2 and 3 (abscissa) to the corresponding anomalies in weeks 4 and 5 (ordinate) across all NDJFM inits; (right) comparison of Z100 polar cap anomalies with Z500 in the subpolar North Atlantic across all NDJFM inits for weeks 2 through 5

sudden stratospheric warming events. Positive anomalies of 500 hPa height averaged over the subpolar North Atlantic (300–359E, 55–90N as in Fig. 7) occur in weeks 1–4 after MJO phase 6 in reanalysis and UFS6 and in weeks 3–5 after MJO phase 4 in UFS5, compared to the relatively low height in weeks 2–5 after MJO phases 2–3 in both prototypes and reanalysis. Both prototypes are able to reproduce the negative phase of NAO in weeks 1–2 following MJO phase 6, though the persistence of the signal is overestimated in UFS6 and underestimated in UFS5. This is consistent with the weakening of polar vortex and the following negative NAM and NAO responses in the troposphere, and corresponds to the positive correlations found in the right column of Fig. 8.

In general, UFS is capable of capturing the Euro-Atlantic teleconnections of the MJO through the stratospheric pathway. Although both prototypes simulate much stronger heat flux responses and a weakening of the polar vortex after a slightly different MJO phase, they are able to reproduce the magnitude of the weakening of the polar vortex and the height responses in both stratosphere and troposphere. Both the upward propagating planetary wave activity and the subsequent downward impacts of the stratospheric polar vortex are successfully captured by both UFS prototypes, which is an improvement compared to previous subseasonal forecasting models (Schwartz and Garfinkel 2020; Stan et al. 2022), though we acknowledge the caveat that the hindcast period used here differs from these previous works.

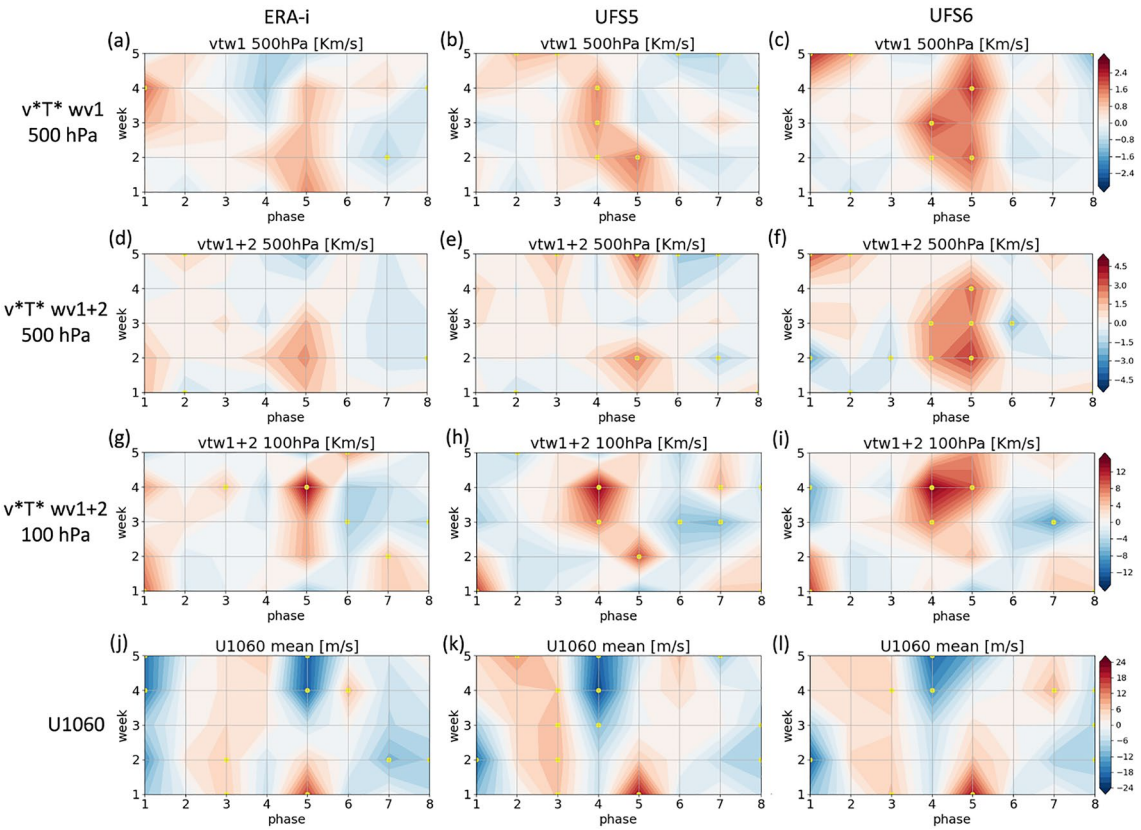

Fig. 9 Meridional heat flux anomalies and zonal-mean zonal wind anomalies in weeks 1–5 following MJO phases 1–8 in November to March. (first row) Wavenumber-1 component of meridional heat flux at 500 hPa, (second row) wavenumber-1 and wavenumber-2 components of meridional heat flux at 500 hPa and (third row) at 100 hPa, and (fourth row) zonal-mean zonal wind at 10 hPa and 60N for ERA-I (left), UFS5 (middle), and UFS6 (right). Yellow dots indicate anomalies statistically significant at the 0.1 level based on bootstrapping

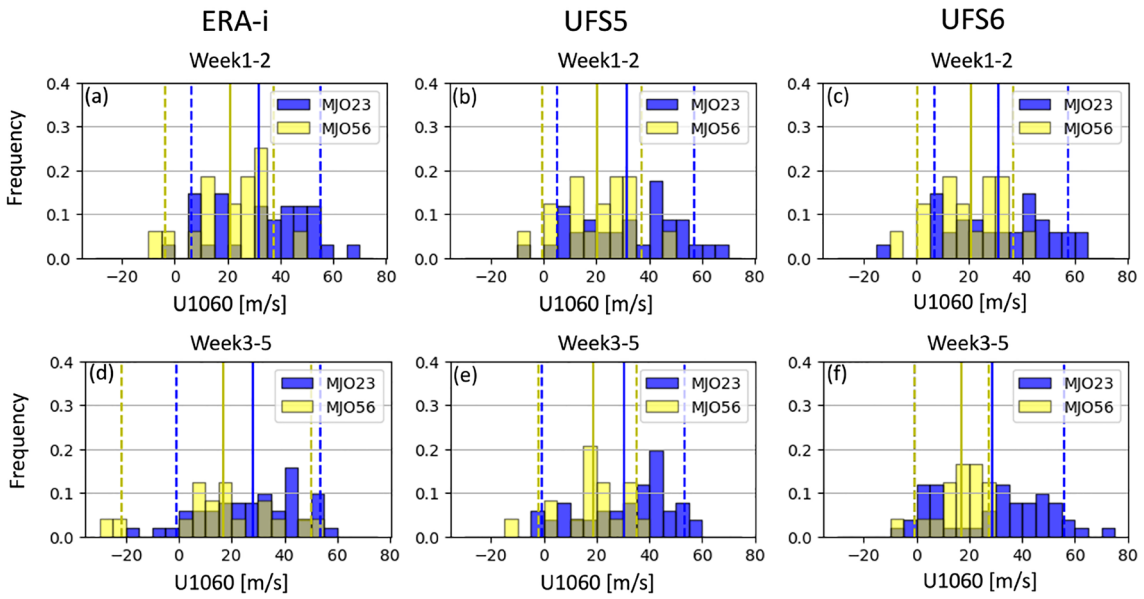

Fig. 10 Histograms of zonal-mean zonal wind at 10 hPa and 60N (U1060) for November-March forecasts for weeks 1–2 (**a**–**c**) and for weeks 3–5 (**d**–**f**) following the MJO phases 2–3 (blue) and phases 5–6 (yellow). The solid blue and yellow lines indicate the mean values of U1060 during phases 2–3 and 5–6, respectively. The dashed blue and yellow lines indicate the 5th and 95th percentile of U1060 during phases 2–3 and 5–6, respectively

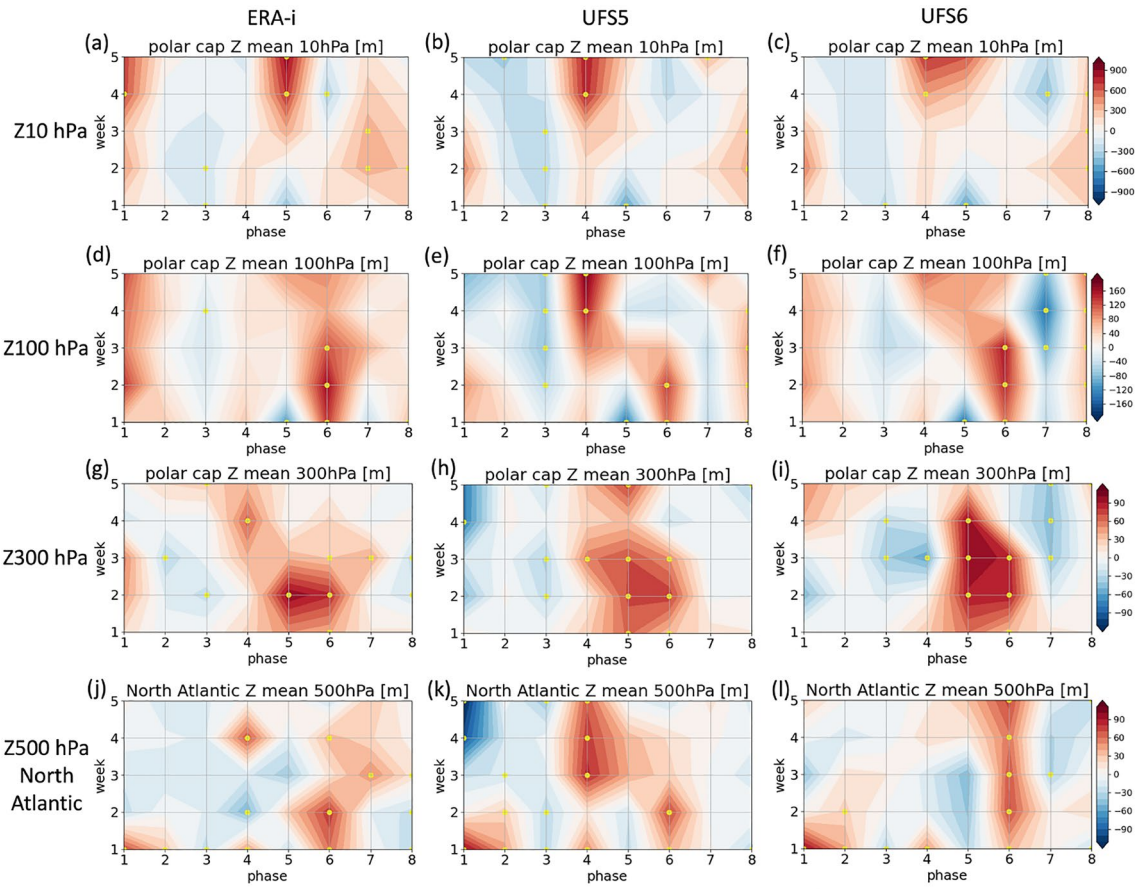

Fig. 11 Geopotential height anomalies in weeks 1–5 following MJO phases 1–8. November-March geopotential height averaged over the polar cap at (first row) 10 hPa, (second row) 100 hPa, (third row) 300 hPa, and (fourth row) averaged over the subpolar North Atlantic at 500 hPa for ERA-I (left), UFS5 (middle), and UFS6 (right). Yellow dots indicate anomalies statistically significant at the 0.1 level based on bootstrapping

3.4 Surface impacts likely arising from the MJO stratospheric pathway

Section 3.3 established that a negative phase of the NAM is exhibited in weeks 1–4 after MJO phase 6 in reanalysis and both prototypes, consistent with the weakening of the polar vortex. It is well-established that a weak vortex and negative NAM typically leads to cold anomalies over Siberia and Northern Europe, and warm anomalies over Eastern Canada and subtropical Eurasia (Garfinkel et al. 2017; King et al. 2019; Baldwin and Dunkerton 2001; Baldwin et al. 2021). We now explore whether the surface temperature impacts following the MJO follow those associated with polar vortex variability more generally.

Figure 12 shows the MJO-induced 2-meter temperature (T2m) response over the Northern Hemisphere in weeks 3–5 after MJO phase 6. Cold anomalies are evident over much of Northern Eurasia in both reanalysis and UFS, consistent with the weak polar vortex and negative NAM conditions evident in Fig. 9 and 11. In contrast, Eastern Canada and Greenland tend to be warmer, though the regional details are different for each panel of Fig. 12. Furthermore, the Eastern United States tends to be anomalously cold, and this feature is captured in UFS5 and displaced northward in UFS6. Finally, negative NAM typically leads to warmth over subtropical Eurasia and the Middle-East, however this feature is prominent primarily in UFS5. Overall, UFS5 simulates a pattern correlation of 0.47 for these subseasonal forecast leads, with most of the error occurring over Western America where the stratospheric route is relatively unimportant. UFS6, on the other hand, simulates overly strong cold over Siberia that is shifted to the west, leading to a relatively lower pattern correlation of 0.26. The overly strong cold anomalies in UFS6 are consistent with the too-persistent NAO response evident in the last row of Fig. 11.

The pattern correlation analysis is summarized in Fig. 13, which also shows the relative amplitude metric (Wang et al. 2020). These metrics are computed for the Eurasian sector only (0–180E, 20–80N). The decrease of the pattern correlation below 0.5 during the second week of the forecast

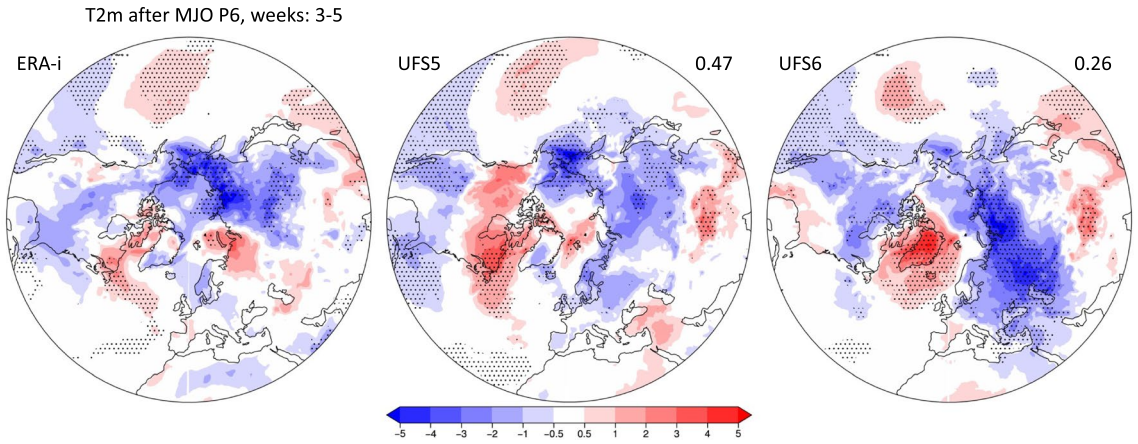

Fig. 12 Composites of T2m daily anomaly in weeks 3–5 after MJO phase 6. Dotted areas denote anomalies statistically significant at the 0.05 level based on a Student t-test. Numbers in the upper right corners show the pattern correlation between reforecasts and ERA-I

(Fig. 13a,b) is similar to other S2S models (Stan et al. 2022). Consistent with Fig. 12, UFS5 better captures the pattern correlation with observations for MJO phase 6 until week 4, however UFS6 performs better afterwards and also for MJO phase 3. The amplitude of the teleconnection in UFS6 is slightly closer to observed values than in UFS5 for MJO phase 3 in week 2 (Fig. 13c), but is overestimated in UFS6 for MJO phase 6 in week 3 (Fig. 13d) consistent with the overly strong cooling in Fig. 12. Overall, UFS5 performs slightly better in capturing the T2m teleconnection over the Euro-Atlantic region for MJO phase 6 through week 3, however the response in week 4 is better predicted in UFS6.

4 Summary and discussion

Stratospheric polar vortex variability and the Madden Julian Oscillation are crucial for providing skillful surface weather predictions on subseasonal to seasonal timescales (Sigmond et al. 2013; Domeisen and Butler 2020; Stan et al. 2022). While these two sources of predictability can act independently to affect surface conditions, in the North Atlantic and Eurasian sectors the surface impacts are co-mingled: recent work has shown that the MJO can affect surface climate over Europe and the North Atlantic at one month lags via the stratosphere (Schwartz and Garfinkel 2017; Green and Furtado 2019; Barnes et al. 2019).

In this work, we assessed whether the UFS protoypes can realistically simulate the impact of the MJO on the North Atlantic surface climate on subseasonal timescales via the stratospheric pathway. A precondition for this is that the models realistically simulate upward and downward stratosphere-troposphere coupling. While previous studies on this topic found that all operational subseasonal forecasting models struggled to represent at least one aspect (and in many cases, most aspects) of this pathway (Schwartz and Garfinkel 2020; Stan et al. 2022), the UFS prototypes are relatively more successful (though we note the caveat that the hindcast period available for UFS differs from that used in previous work). Specifically, the UFS is capable of realistically simulating an enhancement in heat flux in both the troposphere and stratosphere following MJO phase 5, a subsequent weakening of the vortex, downward propagation of the NAM anomaly to the troposphere with a North Atlantic Oscillation imprint, and surface temperature impacts in Eurasia and Eastern North America.

This success of the UFS to capture the MJO stratospheric pathway is a reflection of its ability to capture upward and downward coupling between the troposphere and stratosphere more generally. Specifically, tropospheric and stratospheric stationary waves in the UFS are generally reasonable (though with a too-strong wave-1 and too weak wave-2 in UFS6). Consistent with this, planetary wave heat flux is reasonable in both the troposphere and stratosphere (though with an incorrect ratio of wave-1 vs. wave-2 in UFS6, mirroring its bias in the stationary waves). The stratospheric polar vortex is, if anything, too sensitive to upward propagating wave activity in both prototypes. Downward propagation within the stratosphere is of the correct magnitude, and the lower stratospheric anomaly persists realistically. Finally, anomalous conditions in the polar lower stratosphere lead to a surface response that resembles the North Atlantic Oscillation.

While the UFS appears to be more successful over its hindcast period than any previous modeling system over their hindcast period in simulating the stratospheric MJO teleconnection pathway, we have identified some biases. The ability of the UFS to realistically represent the stratospheric pathway appears to be due to “two wrongs making a right", that is two biases compensating each other for a realistic net

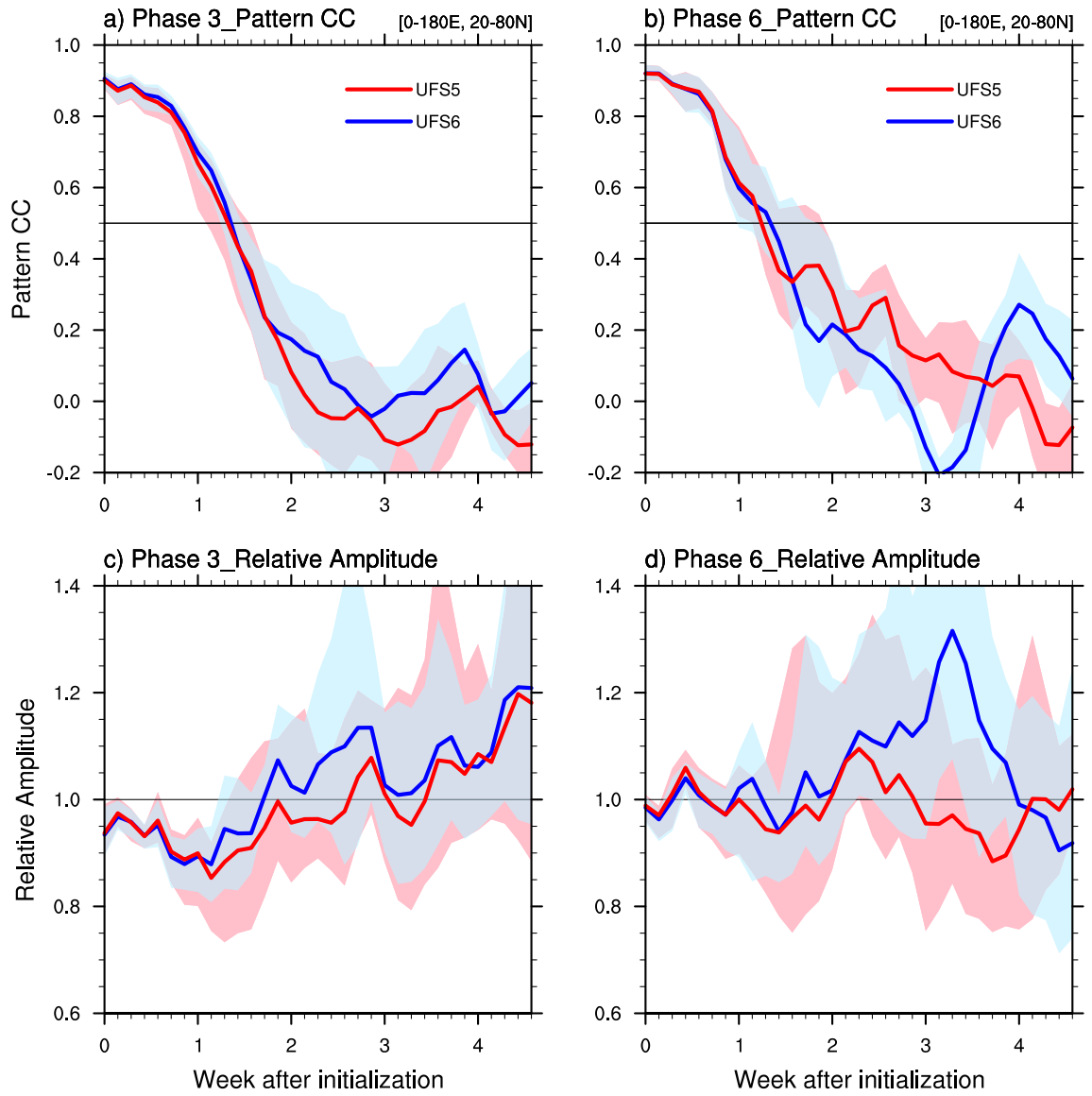

Fig. 13 Pattern correlation coefficient (UFS vs ERA-I) and relative amplitude (UFS/ERA-I) of surface temperature anomalies over Eurasia region (0–180E, 20–80N) vs forecast lead days for the MJO phases (**a**, **c**) 3 and (**b**, **d**) 6. Horizontal solid lines in (**a**) and (**c**) represent the reference line of pattern correlation at 0.5. Horizontal solid lines in (**b**) and (**d**) represent the reference line above (below) which the temperature anomalies are overestimated (underestimated) in UFS models. The gray shading indicates the 95% confidence level determined by the bootstrap test. The lower boundary represents the minimum 2.5th percentile of the bootstrapping distribution between the models, and the upper boundary represents the maximum 97.5th-percentile distribution between the models. The relative amplitude is defined as the T2m anomaly standard deviation in UFS divided by that in ERA-I

response. Specifically, UFS struggles to represent upward wave propagation of wave-2 from the troposphere to the lower stratosphere, but the polar vortex in UFS is also overly sensitive to any heat flux perturbation in the lower stratosphere once it arrives there. The net effect is that UFS6 still represents the stratospheric pathway. However, it is conceivable that fixing one of these biases but not the other may lead to worsened MJO-related predictability and skill.

Paper 1 (Zheng et al. 2024) demonstrated that the MJO propagates too slowly in both prototypes. Further, it demonstrated that the North Pacific response is simulated well in both prototypes, and if anything is too strong in week 3 and 4 in UFS6. A too-slow MJO propagation would, in isolation, tend to enhance the stratospheric pathway (Yadav et al. 2024), and hence fixing it could conceivably weaken the stratospheric pathway. Further, a strong North Pacific teleconnection is a prerequisite for a realistic stratospheric route (Garfinkel et al. 2012, 2014; Schwartz and Garfinkel 2020; Stan et al. 2022), and a weaker North Pacific response would also tend to weaken the stratospheric route. Finally,

there are additional caveats of the UFS prototypes not specifically related to the stratosphere. These caveats are discussed in detail in Paper 1, and are briefly listed here: 1) A relatively short reforecast period (2011–2018) which limits the sample size and preciseness of the computed climatology; 2) Possible impacts from slow-varying climate modes on the results such as El Nino Southern Oscillation (ENSO) and Quasi-Biennial Oscillation (QBO).

One of the motivations for our evaluation of UFS5 as compared to UFS6 is that it offers a relatively clean evaluation of the effect of vertical resolution on stratosphere-troposphere coupling. Namely, UFS6 has nearly double the vertical resolution of UFS5 (Fig. 1). Nevertheless, there is little evidence that UFS6 represents stratosphere-troposphere coupling or the stratospheric pathway of the MJO significantly better than UFS5. This is in contrast to the tropospheric pathway, which was better simulated in UFS6 due an improved subtropical jet (see Paper 1; Zheng et al. 2024). This somewhat perplexing result could be due to a number of reasons

1. Adding resolution but not retuning the scale-dependent parameterizations could lead to poorer overall skill
2. UFS5 already resolves the stratosphere well, and the added value from extra levels (at least in this modeling system) is small and can only be isolated with a longer hindcast period.

Future work should consider these possibilities in more detail.

Acknowledgements This study was supported by the NOAA/OAR Weather Program Office through Grant NA22OAR4590216.

Funding Open access funding provided by Hebrew University of Jerusalem. This study was supported by the NOAA/OAR Weather Program Office through grant NA22OAR4590216. Support from the Swiss National Science Foundation through project PP00P2_198896 to D.D. is gratefully acknowledged.

Data availability ERA-Interim reanalysis is available in https://www.ecmwf.int/en/forecasts/dataset/ecmwf-reanalysis-interim. UFS reforecast data is available on AWS https://registry.opendata.aws/noaa-ufs-s2s/.

Declarations

Conflict of interest The authors have no relevant financial or non-financial interests to disclose.

References

Baldwin MP, Ayarzagüena B, Birner T, Butchart N, Butler AH, Charlton-Perez AJ, Domeisen DI, Garfinkel CI, Garny H, Gerber EP (2021) Sudden stratospheric warmings. Rev Geophys 59(1):2020–000708

Baldwin MP, Dunkerton TJ (2001) Stratospheric harbingers of anomalous weather regimes. Science 294(5542):581–584

Barnes EA, Samarasinghe SM, Ebert-Uphoff I, Furtado JC (2019) Tropospheric and stratospheric causal pathways between the mjo and nao. J Geophys Res Atmos 124(16):9356–9371

Bretherton CS, Widmann M, Dymnikov VP, Wallace JM, Bladé I (1999) The effective number of spatial degrees of freedom of a time-varying field. J Clim 12(7):1990–2009

Butler AH, Arribas A, Athanassiadou M, Baehr J, Calvo N, Charlton-Perez A, Déqué M, Domeisen DI, Fröhlich K, Hendon H (2016) The climate-system historical forecast project: Do stratosphere-resolving models make better seasonal climate predictions in boreal winter? Q J R Meteorol Soc 142(696):1413–1427

Butler AH, Sjoberg JP, Seidel DJ, Rosenlof KH (2017) A sudden stratospheric warming compendium. Earth Syst Sci Data 9(1):63–76

Charlton-Perez AJ, Ferranti L, Lee RW (2018) The influence of the stratospheric state on north atlantic weather regimes. Q J R Meteorol Soc 144(713):1140–1151

Charney JG, Drazin PG (1961) Propagation of planetary-scale disturbances from the lower into the upper atmosphere. J Geophys Res 66(1):83–109

Chwat D, Garfinkel CI, Chen W, Rao J (2022) Which sudden stratospheric warming events are most predictable? J Geophys Res Atmos 127(18):2022–037521

Dee DP, Uppala SM, Simmons AJ, Berrisford P, Poli P, Kobayashi S, Andrae U, Balmaseda M, Balsamo G, Bauer DP (2011) The era-interim reanalysis: configuration and performance of the data assimilation system. Quart J R Meteorol Soc 137(656):553–597

Domeisen DI (2019) Estimating the frequency of sudden stratospheric warming events from surface observations of the north atlantic oscillation. J Geophys Res Atmos 124(6):3180–3194

Domeisen DI, Butler AH (2020) Stratospheric drivers of extreme events at the Earth's surface. Commun Earth Environ 1(1):59

Domeisen DI, Butler AH, Charlton-Perez AJ, Ayarzagüena B, Baldwin MP, Dunn-Sigouin E, Furtado JC, Garfinkel CI, Hitchcock P, Karpechko AY (2020) The role of the stratosphere in subseasonal to seasonal prediction: 2. predictability arising from stratosphere-troposphere coupling. J Geophys Res Atmos 125(2):2019–030923

Domeisen DI, Butler AH, Charlton-Perez AJ, Ayarzagüena B, Baldwin MP, Dunn-Sigouin E, Furtado JC, Garfinkel CI, Hitchcock P, Karpechko AY (2020) The role of the stratosphere in subseasonal to seasonal prediction: 1. predictability of the stratosphere. J Geophys Res Atmos 125(2):2019–030920

Ern M, Preusse P, Gille J, Hepplewhite C, Mlynczak M, Russell J III, Riese M (2011) Implications for atmospheric dynamics derived from global observations of gravity wave momentum flux in stratosphere and mesosphere. J Geophys Res Atmos 116:19

Fromang S, Rivière G (2020) The effect of the madden-julian oscillation on the north atlantic oscillation using idealized numerical experiments. J Atmos Sci 77(5):1613–1635

Garfinkel CI, Benedict JJ, Maloney ED (2014) Impact of the mjo on the boreal winter extratropical circulation. Geophys Res Lett 41(16):6055–6062

Garfinkel CI, Feldstein SB, Waugh DW, Yoo C, Lee S (2012) Observed connection between stratospheric sudden warmings and the Madden–Julian oscillation. Geophys Res Lett 39:18

Garfinkel CI, Hartmann DL, Sassi F (2010) Tropospheric precursors of anomalous northern hemisphere stratospheric polar vortices. J Clim 23(12):3282–3299

Garfinkel C, Schwartz C (2017) Mjo-related tropical convection anomalies lead to more accurate stratospheric vortex variability in subseasonal forecast models. Geophys Res Lett 44(19):10–054

Garfinkel CI, Son S-W, Song K, Aquila V, Oman LD (2017) Stratospheric variability contributed to and sustained the recent hiatus in eurasian winter warming. Geophys Res Lett 44(1):374–382

Green MR, Furtado JC (2019) Evaluating the joint influence of the Madden–Julian oscillation and the stratospheric polar vortex on weather patterns in the northern hemisphere. J Geophys Res Atmos 124(22):11693–11709

Hitchcock P, Shepherd TG, Taguchi M, Yoden S, Noguchi S (2013) Lower-stratospheric radiative damping and polar-night jet oscillation events. J Atmos Sci 70(5):1391–1408

Holton JR (1982) The role of gravity wave induced drag and diffusion in the momentum budget of the mesosphere. J Atmos Sci 39(4):791–799

Jiang Z, Feldstein SB, Lee S (2017) The relationship between the madden-julian oscillation and the north atlantic oscillation. Q J R Meteorol Soc 143(702):240–250

Kim H, Vitart F, Waliser DE (2018) Prediction of the Madden–Julian oscillation: a review. J Clim 31(23):9425–9443. https://doi.org/10.1175/JCLI-D-18-0210.1

King AD, Butler AH, Jucker M, Earl NO, Rudeva I (2019) Observed relationships between sudden stratospheric warmings and european climate extremes. J Geophys Res Atmos 124(24):13943–13961

Kretschmer M, Coumou D, Agel L, Barlow M, Tziperman E, Cohen J (2018) More-persistent weak stratospheric polar vortex states linked to cold extremes. Bull Am Meteor Soc 99(1):49–60

Lawrence ZD, Abalos M, Ayarzagüena B, Barriopedro D, Butler AH, Calvo N, Cámara A, Charlton-Perez A, Domeisen DI, Dunn-Sigouin E (2022) Quantifying stratospheric biases and identifying their potential sources in subseasonal forecast systems. Wea Clim Dyn Discuss 2022:1–37

Limpasuvan V, Hartmann DL, Thompson DW, Jeev K, Yung YL (2005) Stratosphere-troposphere evolution during polar vortex intensification. J Geophys Res Atmos 110:24

Lin H, Brunet G (2018) Extratropical response to the mjo: Nonlinearity and sensitivity to the initial state. J Atmos Sci 75(1):219–234. https://doi.org/10.1175/JAS-D-17-0189.1

Lin H, Brunet G, Fontecilla JS (2010) Impact of the Madden–Julian oscillation on the intraseasonal forecast skill of the north Atlantic oscillation. Geophys Res Lett 37:19

L'Heureux ML, Higgins RW (2008) Boreal winter links between the madden-julian oscillation and the arctic oscillation. J Clim 21(12):3040–3050

Madden RA, Julian PR (1971) Detection of a 4050 day oscillation in the zonal wind in the tropical pacific. J Atmos Sci 28(5):702–708

Scaife AA, Baldwin MP, Butler AH, Charlton-Perez AJ, Domeisen DI, Garfinkel CI, Hardiman SC, Haynes P, Karpechko AY, Lim E-P (2022) Long-range prediction and the stratosphere. Atmos Chem Phys 22(4):2601–2623

Schwartz C, Garfinkel CI (2017) Relative roles of the mjo and stratospheric variability in north Atlantic and European winter climate. J Geophys Res Atmos 122(8):4184–4201

Schwartz C, Garfinkel CI (2020) Troposphere-stratosphere coupling in subseasonal-to-seasonal models and its importance for a realistic extratropical response to the madden-julian oscillation. J Geophys Res Atmos 125(10):2019–032043. https://doi.org/10.1029/2019JD032043‡

Schwartz C, Garfinkel CI, Yadav P, Chen W, Domeisen D (2022) Stationary waves and upward troposphere-stratosphere coupling in s2s models. Wea Clim Dyn 2022:1–25. https://wcd.copernicus.org/articles/3/679/2022/wcd-3-679-2022.html

Sigmond M, Scinocca J, Kharin V, Shepherd T (2013) Enhanced seasonal forecast skill following stratospheric sudden warmings. Nat Geosci 6(2):98–102

Stan C, Zheng C, Chang EK-M, Domeisen DI, Garfinkel CI, Jenney AM, Kim H, Lim Y-K, Lin H, Robertson A (2022) Advances in the prediction of mjo teleconnections in the s2s forecast systems. Bull Am Meteor Soc 103(6):1426–1447

Stefanova L, Meixner J, Wang J, Ray S, Mehra A, Barlage M, Bengtsson L, Bhattacharjee PS, Bleck R, Chawla A, et al (2022) Description and results from ufs coupled prototypes for future global, ensemble and seasonal forecasts at ncep **NCEP Office Notes 510**

Vitart F (2017) Madden–Julian oscillation prediction and teleconnections in the s2s database. Q J R Meteorol Soc 143(706):2210–2220

Vitart F, Ardilouze C, Bonet A, Brookshaw A, Chen M, Codorean C, Déqué M, Ferranti L, Fucile E, Fuentes M (2017) The subseasonal to seasonal (s2s) prediction project database. Bull Am Meteor Soc 98(1):163–173

Wang J, Kim H, Kim D, Henderson SA, Stan C, Maloney ED (2020) Mjo teleconnections over the pna region in climate models. part i: Performance- and process-based skill metrics. J Clim 33(3):1051–1067. https://doi.org/10.1175/JCLI-D-19-0253.1

Weinberger I, Garfinkel CI, Harnik N, Paldor N (2022) Transmission and reflection of upward-propagating rossby waves in the lowermost stratosphere: Importance of the tropopause inversion layer. J Atmos Sci 79(12):3263–3274

Wheeler MC, Hendon HH (2004) An all-season real-time multivariate mjo index: Development of an index for monitoring and prediction. Mon Weather Rev 132(8):1917–1932

Yadav P, Garfinkel CI, Domeisen DI (2024) The role of the stratosphere in teleconnections arising from fast and slow mjo episodes. Geophys Res Lett 51(1):2023–104826

Zheng C, Domeisen DIV, Garfinkel CI, Jenney AM, Kim H, Wang J, Wu Z, Stan C (2024) The impact of vertical model levels on the prediction of mjo teleconnections part i: the tropospheric pathways in the ufs global coupled model. Clim Dyn. https://doi.org/10.1007/s00382-024-07377-x

Authors and Affiliations

Chaim I. Garfinkel[1] · Zheng Wu[2,3] · Priyanka Yadav[2,4] · Zachary Lawrence[5] · Daniela I. V. Domeisen[2,6] · Cheng Zheng[7] · Jiabao Wang[8] · Andrea M. Jenney[9] · Hyemi Kim[10] · Chen Schwartz[1,11] · Cristiana Stan[12]

✉ Chaim I. Garfinkel
chaim.garfinkel@mail.huji.ac.il

Zheng Wu
zwu26@albany.edu

Priyanka Yadav
pyadav@umd.edu

Zachary Lawrence
zachary.lawrence@noaa.gov

Daniela I. V. Domeisen
daniela.domeisen@unil.ch

Cheng Zheng
czheng@ldeo.columbia.edu

Jiabao Wang
jiw093@ucsd.edu

Andrea M. Jenney
andrea.jenney@oregonstate.edu

Hyemi Kim
hyemi.kim@stonybrook.edu

Chen Schwartz
chen.schwartz1@mail.huji.ac.il

Cristiana Stan
cstan@gmu.edu

[1] The Fredy and Nadine Hermann Institute of Earth Sciences, Hebrew University of Jerusalem, Givat Ram, Jerusalem, Israel

[2] Institute for Atmospheric and Climate Science, ETH Zürich, Zürich, Switzerland

[3] Department of Atmospheric and Environmental Sciences, University at Albany, SUNY, Albany, USA

[4] Earth System Science Interdisciplinary Center, University of Maryland, College Park, MA, USA

[5] Physical Science Laboratory, NOAA, Boulder, Colorado, USA

[6] Faculty of Geosciences and Environment, University of Lausanne, Lausanne, Switzerland

[7] Lamont-Doherty Earth Observatory, Columbia University, Palisades, NY, USA

[8] Center for Western Weather and Water Extremes, Scripps Institute of Oceanography, University of California, San Diego, CA, USA

[9] College of Earth, Ocean, and Atmospheric Sciences, Oregon State University, Corvallis, OR, USA

[10] School of Marine and Atmospheric Sciences, Stony Brook University, Stony Brook, NY, USA

[11] Centre for Climate Research Singapore, Singapore, Singapore

[12] Department of Atmospheric, Oceanic and Earth Sciences, George Mason University, Fairfax, VA, USA